Journal of Alloys and Compounds 588 (2014) 305–309

Contents lists available at ScienceDirect

Journal of Alloys and Compounds

journal homepage: www.elsevier.com/locate/jalcom

Synthesis of porous zinc aluminate spinel ($ZnAl_2O_4$) by metal-chitosan complexation method

Fabiane Marconato Stringhini [a], Edson Luiz Foletto [a,*], Daniela Sallet [a], Daniel Assumpção Bertuol [a], Osvaldo Chiavone-Filho [b], Claudio Augusto Oller do Nascimento [c]

[a] Department of Chemical Engineering, Federal University of Santa Maria, 97105-900 Santa Maria, Brazil
[b] Department of Chemical Engineering, Federal University of Rio Grande do Norte, 59078-970 Natal, Brazil
[c] Department of Chemical Engineering, University of São Paulo, 05424-970 São Paulo, Brazil

ARTICLE INFO

Article history:
Received 7 September 2013
Received in revised form 23 October 2013
Accepted 13 November 2013
Available online 21 November 2013

Keywords:
Zinc aluminate
$ZnAl_2O_4$
Synthesis
Metal-chitosan complexation

ABSTRACT

Zinc aluminate ($ZnAl_2O_4$) particles with a spinel structure were prepared by metal-chitosan complexation method. The solids were obtained by the thermal decomposition of precursor compound of metallic hydroxides mixture and the biopolymer chitosan. X-ray diffraction analysis (XRD), Fourier transform infrared spectroscopy (FTIR), X-ray fluorescence (XRF), scanning electron microscopy (SEM) and N_2-adsorption–desorption isotherms were used for the characterization of the products. The results showed that the $ZnAl_2O_4$ spinel can be obtained by heating the precursor at temperatures above of 500 °C, resulting in a material with porous structure and large surface area and high purity.

1. Introduction

Zinc aluminate ($ZnAl_2O_4$) is a ternary oxide semiconductor of the form AB_2O_4, in which A represents a divalent metallic cation that usually occupies a tetrahedral site and B represents trivalent metallic cations that normally occupy the octahedral sites of a cubic structure [1]. $ZnAl_2O_4$ is of interest due to its combination of desirable properties such as high mechanical resistance, high thermal stability, low temperature sinterability, low surface acidity and better diffusion [2–5]. Therefore, it is used as high temperature ceramic material, optical coating or host matrix but most importantly as catalyst or catalyst support [6,7]. Also $ZnAl_2O_4$ is a semiconductor suitable for ultraviolet (UV) photoelectronic application [8].

In recent years, $ZnAl_2O_4$ has been largely used as catalyst and catalyst support in several reactions such as photodegradation of dye [9], alkylation of 2-hydroxypyridine with methanol [10], ethanol steam reforming [11], hydroformylation and hydrogenation [12], iso-butane combustion [13], combustion of soot under NO_x/O_2 atmosphere [14], selective hydrogenation of o-chloronitrobenzene [15], transesterification of vegetable oil [16], acetylation of amines, alcohols and phenols [17] and degradation of gaseous toluene [18]. The high surface area and a porous structure of $ZnAl_2O_4$ are of great importance for catalytic purposes. Therefore, in the present study, an attempt is given to synthesize single phase and mesoporous $ZnAl_2O_4$ with high specific surface area by the microwave assisted hydrothermal method. There are many methods of preparation of $ZnAl_2O_4$ oxide, such as co-precipitation [19], modified citrate [20], microwave-hydrothermal [6], solid-state reaction [21], hydrothermal [22], sol–gel [23], and polymeric precursor [24]. Recently, a novel method has been developed with the purpose of obtaining solid materials with porous structure and high surface area, called metal-chitosan complexation method. The method consists of obtaining hybrid particles compound of metallic hydroxides mixture and the biopolymer chitosan. Through the polymer elimination by thermal treatment a porous particle is obtained. Chitosan has been used in the preparation other materials such as magnesium aluminate ($MgAl_2O_4$) [25], magnesium oxide (MgO) [26], alumina (Al_2O_3) [27], ceria (CeO_2) [28] and silica (SiO_2) [29].

In this context, the aim in this work is to prepare porous $ZnAl_2O_4$ particles with high surface area by an alternative method, i.e., the metal-chitosan complexation method. The influence of the calcination temperature on its physical properties was investigated. The powders produced were characterized by the following techniques: X-ray diffraction (XRD), scanning electron microscopy (SEM), infrared spectroscopy (FTIR), X-ray fluorescence (XRF) and N_2-adsorption–desorption isotherms.

* Corresponding author. Tel.: +55 55 32208448; fax: +55 55 32208030.
E-mail address: efoletto@gmail.com (E.L. Foletto).

0925-8388/$ - see front matter © 2013 Elsevier B.V. All rights reserved.
http://dx.doi.org/10.1016/j.jallcom.2013.11.078

2. Experimental

2.1. Synthesis procedure for the $ZnAl_2O_4$ particles

The synthesis procedure carried out in this work was similar to the previously developed synthesis of magnesium aluminate ($MgAl_2O_4$) [25]. For the $ZnAl_2O_4$ synthesis by metal-chitosan complexation route, 11.88 g of $Zn(NO)_3.6H_2O$ (Vetec, analytical grade, purity >99%) were dissolved in 20 mL distilled water, 31.5 g of $Al(NO_3)_3{\cdot}9H_2O$ (Vetec, analytical grade, purity >99%) were dissolved in 30 mL distilled water and 9.84 g of chitosan polymer $[(C_6H_{11}O_4N)_n]$ (Purifarma) were dissolved in 317 mL of acetic acid solution (5% v/v). The Zn and Al aqueous solutions were then added to the polymer solution with magnetic stirring. The Zn–Al–chitosan solution was added dropwise with a peristaltic pump to a NH_4OH solution (50%, v/v) under vigorous stirring. After adding the solutions, the system was kept under stirring for 3 h to complete the gelification process. The gel spheres were separated from the solution and further dried at ambient temperature for 48 h. This material was calcined in an oxidizing atmosphere (air) at temperatures of 500 – 900 °C, for 4 h, to eliminate the organic matter and to form the ternary oxide.

2.2. Characterization techniques

The surface physical morphology was examined with a scanning electron microscope (SEM, Shimadzu SSX-550). The powders produced were characterized in a X-ray diffractometer (equipment Bruker D8 Advance, with Cu Kα radiation, $\lambda = 0.15405$ nm). The crystallite size of these samples was estimated using the Scherrer's formula [30] (using silicon as standard) which is written follow, applied to the peak at $2\Theta = 36.75°$ (see XRD in Fig. 1); $d = 0.9\lambda/B\cos\Theta$, where d is the average crystallite size, λ is the wavelength of X-ray, B is the peak width at half maximum height and Θ the Bragg's angle. The N_2 adsorption–desorption isotherm measurements were carried out at 77 K using an ASAP 2020 apparatus. Specific surface areas were calculated according to the Brunauer–Emmett–Teller (BET) method, and the pore size distributions were obtained according to the Barret–Joyner–Halenda (BJH) method from the adsorption data. FTIR spectra were recorded on a PerkinElmer FTIR Spectrum spectrophotometer in the region of 375–4000 cm^{-1}, using KBr pellets. Chemical composition of the powders was determined by X-ray fluorescence (EDX-750, Shimadzu) spectrometry.

3. Results and discussion

XRD was used to investigate the phase structure and average crystallite size of the $ZnAl_2O_4$ spinel. Fig. 1 shows typical XRD patterns of zinc aluminate ($ZnAl_2O_4$) powder obtained at a calcination temperature of 500 – 900 °C. According to the XRD patterns, all diffraction peaks can be perfectly indexed as centered cubic spinel-structured $ZnAl_2O_4$ (JCPDS Card No. 05-0669). The intensities and positions of the peaks of the synthesized powders are in agreement with those of reference (JCPDS Card No. 05–0669). The characteristic peaks at 2Θ of 31.2°, 36.75°, 44.7°, 49.1°, 55.6° and 59.3° are corresponding to (220), (311), (400), (331), (422) and (511) and (440) diffraction planes. No other peak of any phase was detected. It can be seen that the widths of peaks for the samples obtained at lower temperatures are broader, indicating that the crystallite size is very small. It can be seen also that increasing the calcination temperature, the width of peaks becomes narrower. It is associated with the increase of the crystallite size. The average crystallite size was estimated by applying the Scherrer equation on the peak at $2\Theta = 36.75°$ for all samples. The average crystallite size for all the samples is shown in Table 1. The crystallite size found for all samples was very small, with values between 3.60 and 7.91 nm.

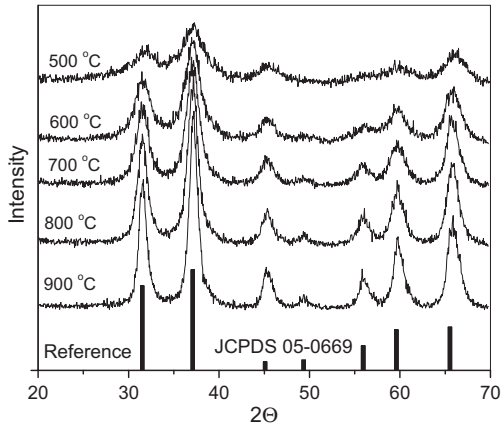

Fig. 1. XRD patterns of the samples obtained by different calcination temperatures and the JCPDS Card No. 05-0669.

Chemical compositions determined by X-ray fluorescence technique for the powders are listed in Table 1. The results reveal that only minor undesirable substances remained in the synthesized powders. The obtained powders contains less than c.a. 1.0 wt.% impurities, which were iron, calcium, nickel and sulfur. These impurities may be present in the nitrate salts, i.e., zinc nitrate and aluminum nitrate, used as reagents in the synthesis. Therefore, the $ZnAl_2O_4$ powders obtained by metal-chitosan complexation method were of high purity grade.

FTIR was applied in this work to characterize the interaction of chitosan with Zn and Al ions, and to confirm the formation of spinel structure, $ZnAl_2O_4$. It is known that chitosan has the ability to form complexes with metallic ions due to the presence of potentially reactive functional groups in its structure such as amine groups, hydroxyl groups attached to primary and secondary carbons and also some acetamide groups [25,29,31]. From Fig. 2, it can be seen that the FTIR spectrum of the Zn–Al–chitosan complex (before calcination) (Fig. 2b) exhibits characteristic bands of chitosan, according to Fig 2a. The corresponding bands of chitosan are located at 2900 cm^{-1}, associated to N–H vibration, 1665 cm^{-1}, associated to acetyl groups (C═O) in chitosan, 1380 cm^{-1}, attributed to amide III (combination of N–H deformation and C–N stretching) and at 1063–1043 cm^{-1}, corresponding to C–O vibration [28]. The band in the region of 3400 cm^{-1} is associated with the stretch of OH groups overlapped by the stretch of chitosan polymer [25]. The change in band intensities observed between chitosan and Zn–Al–chitosan complex suggests that the Zn and Al ions interact with these functional groups during metal–polymer complex formation. An intense absorption band is located in the range of 1000–400 cm^{-1} (Fig. 2b), which can be attributed to the vibrational modes of different groups corresponding to N–H, M–O–M and M–O (M = Zn or Al) [31]. The increase in the intensity of the band at 1380 cm^{-1} in the spectrum of the Zn–Al–chitosan sample is due to the strong interaction of (Zn–Al) metals with the amine groups of the polymer bound to the glycoside ring. In Fig. 2(c–f) it is shown the FTIR spectra for the calcined samples from 500 to 900 °C. An important difference can be observed in the characteristic bands between Zn–Al–chitosan complex sample and calcined samples. The spectra of all the calcined samples exhibited a common broad band near 3450 cm^{-1} and near 1640 cm^{-1} due to the -OH stretching vibrations and deformation vibration of water molecules respectively. The bands between 450 and 700 cm^{-1} confirm the formation of spinel structure, $ZnAl_2O_4$, according the XRD analysis (Fig. 1). These bands are typical of Zn–O and Al–O bonds which built up the $ZnAl_2O_4$ spinel and indicate its formation for all the synthesized samples [32].

Fig. 3 shows the nitrogen adsorption–desorption isotherms (Fig. 3a) and the corresponding pore size distribution (Fig. 3b) of

Table 1
Chemical composition of the synthesized samples, expressed in wt%.

Sample/Constituent (°C)	$ZnAl_2O_4$	Fe_2O_3	CaO	NiO	SO_3
500C	98.92	0.62	0.27	0.11	0.08
600	98.97	0.43	0.35	0.15	0.10
700	99.00	0.45	0.33	0.14	0.09
800	98.92	0.51	0.43	0.14	–
900	99.02	0.39	0.37	0.12	0.10

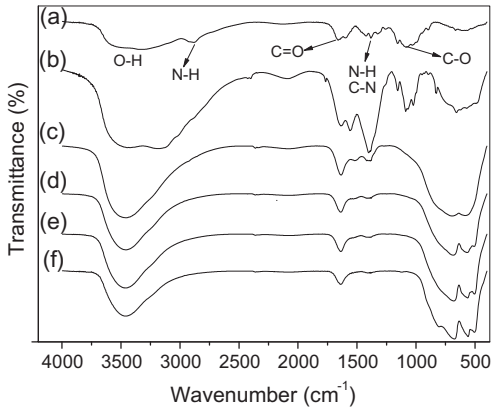

Fig. 2. FTIR spectra for (a) chitosan, (b) spheres (Zn–Al–chitosan complex) dried at room temperature for 48 h and spheres calcined at (c) 500, (d) 600, (e) 700 and (f) 900 °C.

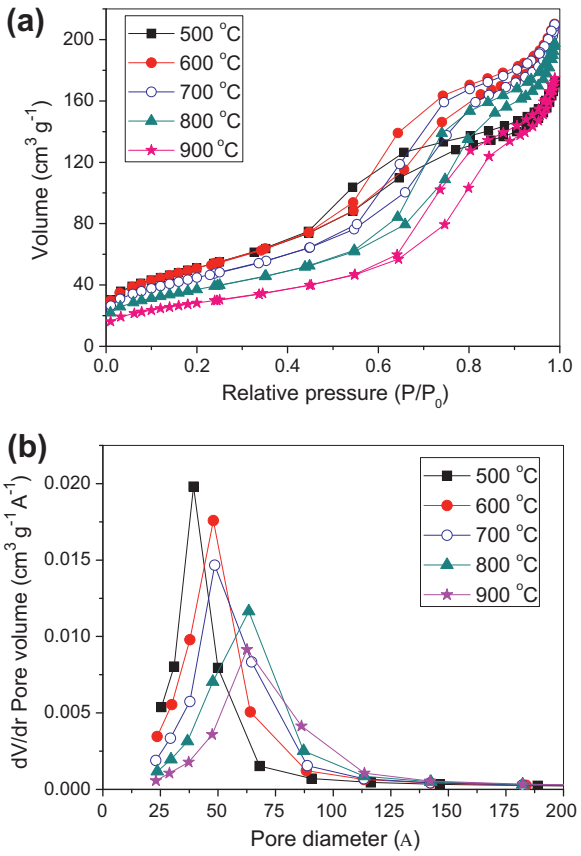

Fig. 3. (a) Nitrogen adsorption–desorption isotherms and (b) pore size distribution of the samples obtained by different calcination temperatures.

zinc aluminate powders calcined at different temperatures. The adsorption–desorption isotherms are similar in behavior in all samples, and according to IUPAC classification [33] are type IV, presenting a hysteresis loop that indicate the presence of mesoporosity. The presence of mesoporous was confirmed by analysis of pore size distribution (Fig. 3b), which shows spectra of pore diameter in the mesoporous region for the all samples (20 Å < pore diameter <500 Å) according to the IUPAC classification [33]. In addition, the pore size distribution of these samples are uniform and unimodal, with maxima in the range of 40–60 Å, corresponding

Table 2
Surface area, average crystallite size, and pore parameters of $ZnAl_2O_4$ particles synthesized by different temperatures.

Sample (°C)	Crystallite size (nm)	Surface area ($m^2\ g^{-1}$)	Total pore volume ($cm^3\ g^{-1}$)	Average pore size (Å)
500	3.60	184.55	0.283	56.67
600	4.68	184.90	0.337	62.90
700	5.00	162.25	0.333	69.51
800	6.76	134.12	0.311	78.80
900	7.91	103.10	0.274	90.05

to a variety of accumulated pore voids among particles [34,35]. It can be seen from Fig. 3b that the maxima and width of the pore size distribution increase with the calcination temperature.

Surface and pore properties of the $ZnAl_2O_4$ particles calcined at different temperatures are presented in Table 2. The data concerning pore size indicate that the pore size increases significantly with the reaction time, although the total pore volume was not practically altered. All samples were characterized by high total pore volume, and the samples obtained at higher calcination temperatures, by high average pore size. Important values concerning surface area were obtained. High surface areas were obtained for the samples calcined at 500 and 600 °C (184 $m^2\ g^{-1}$ for both), and also for the sample calcined at 700 °C (162 $m^2\ g^{-1}$). It was also observed that the surface area significantly decreases at higher calcination temperatures. For example, at 900 °C, there was a reduction of about 85% in surface area value in comparison to the samples prepared in the temperatures of 500 and 600 °C.

In Table 3, a comparison among some physical properties of $ZnAl_2O_4$ particles prepared by different routes is presented. From Table 3, it can be seen that each method results in $ZnAl_2O_4$ particles with different physical characteristics. Despite microwave [6,9] hydrothermal [9] and citrate [20] routes generate particles with higher surface area, the method proposed in this work also resulted in a material with high surface area, comparable and superior than the ones obtained by other routes, including some methods such as hydrothermal, microwave and citrate performed in other specific conditions, as listed in Table 3. The metal-chitosan complexation method results in a combination of intrinsic characteristics and desirable for catalytic purposes such as high pore volume and pore size, i.e., high porosity, and small crystallite size. In addition, the synthesis route proposed is easier and simpler because it doesn't need a sophisticate energy source as microwave and also closed vessel at high pressure for the synthesis as in the case of hydrothermal and hydrothermal-microwave routes.

Scanning electron microscopy (SEM) was carried out in order to observe the morphologies of the different samples obtained. The SEM images shown in Fig. 4 exhibit images of the (a) external surface of the sphere dried at room temperature for 48 h, (b) external surface of the sphere calcined at 500 °C, (c) internal surface of the sphere calcined at 500 °C, and (d) internal surface of the sphere calcined at 900 °C. In Fig. 4a it can be observed that the sphere surface is rough but free of cracks. The average sphere diameter determined by SEM was of about 2–3 mm. In Fig. 4b cracks caused by the calcination process are observed. During the calcination process the decomposition of organic matter (chitosan) occurs, then, pore formation occurs as the volatile substances are eliminated [31]. In Fig. 4c and d it is possible to observe the internal porosity of the sphere. In addition, the sphere calcined at 500 °C (Fig. 4c) shows smaller cavities than the sphere calcined at 900 °C (Fig. 4d), which is in agreement with the results obtained in the characterization concerning to the pore size as shown in Table 1.

Table 3
Comparison of some physical properties of $ZnAl_2O_4$ particles prepared by different methods.

Synthesis method	Surface area ($m^2\ g^{-1}$)	Mean crystallite size (nm)	Average pore size (Å)	Total pore volume ($cm^3\ g^{-1}$)	Reference
Metal-chitosan complexation	103–185	3.6–7.9	56–90	0.274–0.337	This work
Co-precipitation	22.36	482	–	–	[36]
Co-precipitation	86	8	–	–	[17]
Co-precipitation	94.4	12.93	98.5	0.261	[9]
Co-precipitation	160	~50	–	0.38	[37]
Alkoxide route	126	28	–	–	[38]
Sol–gel technique	58	15–20	58	0.029	[39]
Citrate technique	230	5–8	36	0.22	[20]
Citrate technique	73.5	10.2	40–70	0.157	[18]
Hydrothermal	165.5	14.6	80	–	[22]
Hydrothermal	127.6	12.1	70	0.286	[18]
Hydrothermal	99	10	54	0.16	[40]
Hydrothermal	254.7	17.7	38.2	0.092	[9]
Solvothermal	165.5	14.6	20	0.312	[18]
Solvothermal	180	~50	–	~0.2	[37]
Microwave-solvothermal	133	6	48	0.18	[14]
Microwave-solvothermal	140	~50	–	~0.2	[37]
Microwave-hydrothermal	220	11.2	<10	0.135	[6]
Microwave-hydrothermal	279.7	10	82.1	0.626	[9]
Modified sol–gel method	40.45	26.82	148.7	0.15	[32]
Epoxide driven sol–gel route	160	11	28.9	0.446	[41]
Combustion method	20.7	14.5	–	–	[42]
Combustion method	17.3	–	–	0.023	[43]

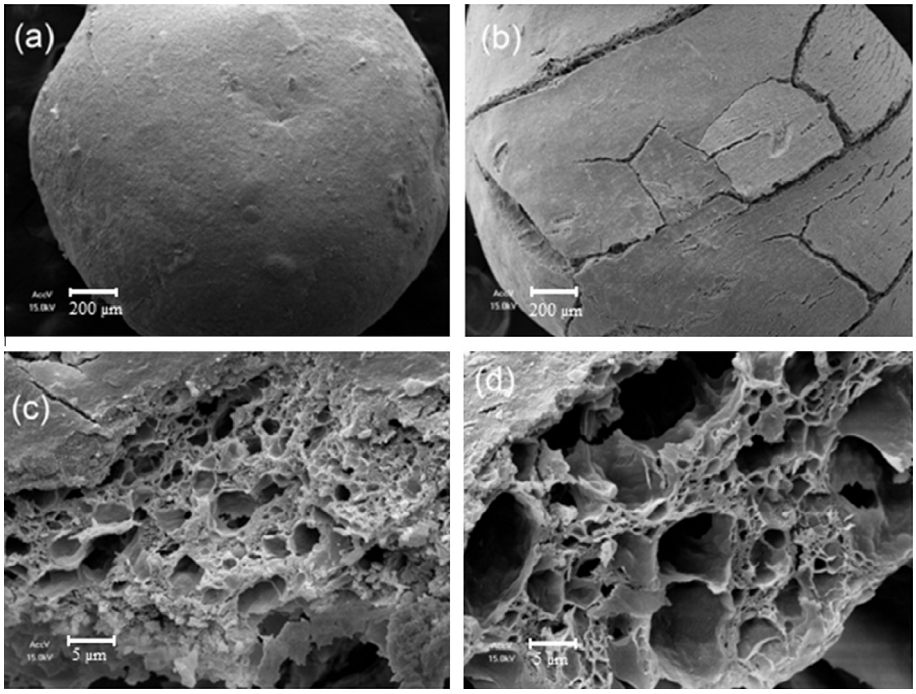

Fig. 4. SEM images of the (a) external surface of the sphere dried at room temperature for 48 h, (b) external surface of the sphere calcined at 500 °C, (c) internal surface of the sphere calcined at 500 °C and (d) internal surface of the sphere calcined at 900 °C.

4. Conclusions

$ZnAl_2O_4$ solid were obtained successfully from metal-chitosan complexation method. From metal-chitosan complexation route, a spinel phase can be obtained at temperatures above 500 °C. A material with porous structure, large surface area and high purity was obtained. The method presented in this work leads to the obtainment of materials with important properties for application in the field of catalysis and in separation processes.

Acknowledgements

Brazilian financial support provided by CAPES (Coordenação de Aperfeiçoamento de Pessoal de Nível Superior) is gratefully acknowledged.

References

[1] E.H. Walker Jr., J.W. Owens, M. Etienne, D. Walker, Mater. Res. Bull. 37 (2002) 1041–1050.

[2] M. Nilsson, K. Jansson, P. Jozsa, L.J. Pettersson, Appl. Catal. B: Environ. 86 (2009) 18–26.
[3] J. Wrzyszcz, M. Zawadzki, A.M. Trzeciak, J.J. Ziółkowski, J. Molec, Catal. A: Chem. 189 (2002) 203–210.
[4] M. Zawadzki, W. Mišta, L. Kępiński, Vacuum 63 (2001) 291–296.
[5] A.R. Phani, M. Passacantando, S. Santucci, Mater. Chem. Phys. 68 (2001) 66–71.
[6] M. Zawadzki, Solid State Sci. 8 (2006) 14–18.
[7] H. Dixit, N. Tandon, S. Cottenier, R. Saniz, D. Lamoen, B. Partoens, V. Van Speybroeck, M. Waroquier, New J. Phys. 13 (2011), http://dx.doi.org/10.1088/1367-2630/13/6/063002.
[8] Y. Wang, Q. Liao, H. Lei, X.P. Zhang, X.C. Ai, J.P. Zhang, K. Wu, Adv. Mater. 18 (2006) 943–947.
[9] E.L. Foletto, S. Battiston, J.M. Simões, M.M. Bassaco, L.S.F. Pereira, É.M.M. Flores, E.I. Müller, Microp. Mesop. Mater. 163 (2012) 29–33.
[10] H. Grabowska, M. Zawadzki, L. Syper, Appl. Catal. A: Gen. 314 (2006) 226–232.
[11] A.E. Galetti, M.F. Gomez, L.A. Arrúa, M.C. Abello, Appl. Catal. A: Gen. 380 (2010) 40–47.
[12] M. Lenarda, M. Casagrande, E. Moretti, L. Storaro, R. Frattini, S. Polizzi, Catal. Lett. 114 (2007) 79–84.
[13] W. Staszak, M. Zawadzki, J. Okal, J. Alloys Comp. 492 (2010) 500–507.
[14] M. Zawadzki, W. Staszak, F.E.L. Suárez, M.J.I. Gómez, A.B. López, Appl. Catal. A: Gen. 371 (2009) 92–98.
[15] G. Fan, J. Wang, F. Li, Catal. Commun. 15 (2011) 113–117.
[16] V. Pugnet, S. Maury, V. Coupard, A. Dandeu, A.A. Quoineaud, J.L. Bonneau, D. Tichit, Appl. Catal. A: Gen. 374 (2010) 71–78.
[17] S. Farhadi, S. Panahandehjoo, Appl. Catal. A: Gen. 382 (2010) 293–302.
[18] X. Li, Z. Zhu, Q. Zhao, L. Wang, J. Hazard. Mater. 186 (2011) 2089–2096.
[19] T.K. Parya, R.K. Bhattacharyya, S. Banerjee, U.B. Adhikari, Ceram. Int. 36 (2010) 1211–1215.
[20] L. Chen, X. Sun, Y. Liu, K. Zhou, Y. Li, J. Alloys Comp. 376 (2004) 257–261.
[21] L. Zou, F. Li, X. Xiang, D.G. Evans, X. Duan, Chem. Mater. 18 (2006) 5852–5859.
[22] Z. Zhu, X. Li, Q. Zhao, S. Liu, X. Hu, G. Chen, Mater. Lett. 65 (2011) 194–197.
[23] M.T. Tsai, Y.S. Chang, I.B. Huang, B.Y. Pan, Ceram. Int. 39 (2013) 3691–3697.
[24] L. Gama, M.A. R, B.S. Barros, R.H.A. Kiminami, I.T. Weber, A.C.F.M. Costa, J. Alloys Comp. 483 (2009) 453–455.
[25] G.D.B. Nuernberg, E.L. Foletto, L.F.D. Probst, C.E.M. Campos, N.L.V. Carreño, M.A. Moreira, Chem. Eng. J. 193–194 (2012) 211–214.
[26] I. Almerindo, L.F.D. Probst, C.E.M. Campos, R.M. Almeida, S.M.P. Meneghetti, M.R. Meneghetti, J.M. Clacens, H.V. Fajardo, J. Power Sour. 196 (2011) 8057–8063.
[27] R.M. Almeida, H.V. Fajardo, D.Z. Mezalira, G.B. Nuernberg, L.K. Noda, L.F.D. Probst, N.L.V. Carreño, J. Mol. Catal. A: Chem. 259 (2006) 328–335.
[28] A.B. Sifontes, G. Gonzalez, J.L. Ochoa, L.M. Tovar, T. Zoltan, E. Cañizales, Mater. Res. Bull. 46 (2011) 1794–1799.
[29] T.P. Braga, E.C.C. Gomes, A.F. Sousa, N.L.V. Carreño, E. Longhinotti, A. Valentini, J. Non-Cryst. Sol. 355 (2009) 860–866.
[30] B.D. Cullity, S.R. Stock, Elements of X-Ray Diffraction, third ed., Prentice-Hall Inc., 2001.
[31] T.P. Braga, E. Longhinotti, A.N. Pinheiro, A. Valentini, J. Appl. Catal. A: Gen. 362 (2009) 139–146.
[32] R.T. Kumar, N.C.S. Selvam, C. Ragupathi, L.J. Kennedy, J.J. Vijaya, Powder Technol. 224 (2012) 147–154.
[33] International Union of Pure and Applied Chemistry, IUPAC, Pure Appl. Chem. 57 (1985) 603.
[34] G. Collazzo, S.L. Jahn, N.L. Carreñno, E.L. Foletto, Braz. J. Chem. Eng. 28 (2011) 265–272.
[35] E.L. Foletto, J.M. Simões, M.A. Mazutti, S.L. Jahn, E.I. Muller, L.S.F. Pereira, E.M.M. Flores, Ceram. Int. 39 (2013) 4569–4574.
[36] Z. Chen, E. Shi, Y. Zheng, W. Li, N. Wu, W. Zhong, Mater. Lett. 56 (2002) 601–605.
[37] W. Walerczyk, M. Zawadzki, J. Okal, Appl. Surf. Sci. 257 (2011) 2394–2400.
[38] C.O. Arean, B.S. Sintes, G.T. Palomino, C.M. Carbonell, E.E. Platero, J.B. Soto, Micropor. Mater. 8 (1997) 187–192.
[39] X. Wei, D. Chen, Mater. Lett. 60 (2006) 823–827.
[40] H. Grabowska, M. Zawadzki, L. Syper, Appl. Catal. A: Gen. 265 (2004) 221–227.
[41] M. Davis, C. Gümeci, R. Alsup, C. Korzeniewski, L.J. Hope-Weeks, Mater. Lett. 73 (2012) 139–142.
[42] D. Visinescu, B. Jurca, A. Ianculescu, O. Carp, Polyhedron 30 (2011) 2824–2831.
[43] C.T. Alves, A.S. Oliveira, S.A.V. Carneiro, R.C.D. Santos, S.A.B.V. Melo, H.M.C. Andrade, F.C. Marques, E.A. Torres, Proc. Eng. 42 (2012) 1928–1945.